Design and Analysis of an Interactive Motion Simulator in Space Entertainment System

Kuei-Shu Hsu[1], Wei-Ting Cho[2], Chin-Feng Lai[1], Xiaofei Wang[3] and Yueh-Min Huang[12]
[1]Department of Applied Geoinformatics, Chia Nan University of Pharmacy & Science
Tainan 701, Taiwan
[2]Department of Engineering Science, National Cheng Kung University
Taiwan 701, Taiwan
[3]School of Computer Science and Engineering, Seoul National University
Seoul, 151-742, South Korea
[e-mail: huang@mail.ncku.edu.tw]

Abstract

In this paper, the analysis and design of a motion simulator (based on the approach taken by interactive virtual reality (VR) entertainment systems) is conducted. The main components of the system include a bilateral control interface, simulation and a motion simulator control scheme. The space entertainment system uses a virtual environment that enables operators to feel the actual feedback sensing and distorted motion from the virtual environment, just as they would in the real environment. The space entertainment system integrates the dynamics of the motion simulator and the virtual environment and the operator maneuvers a steering wheel to interact with the system. The multiple bilateral control schemes employ a dynamical controller, which is designed by considering the velocity and acceleration that the operator imposes on the joystick, the environmental changes imposed on the motion simulator. In addition, we develop a calculated method to evaluate the Ratio of the simulation results. It is shown that the proposed control scheme can improve the performance of the visual entertainment system. Experiments are conducted on the virtual reality entertainment system to validate the theoretical developments.

1. Introduction

Many industry aviation, medicine, nuclear systems for manufacturing in hazardous areas such as nuclear sites, for training pilots with in-flight simulators, etc. [1], and latest experiences have shown the symbiosis of virtual reality (VR) techniques can work satisfactorily. VR with a haptic property offers the chance to build simulation models for the operator for controlling the remote systems. The interaction between the operators and telerobotics for remote and distant control processes is achieved by employing some specified telemechanism that can copy human actions at the end-effector to carry out a task and vice versa [2-4]. An example of such processes is telerobotic systems in a virtual environment with a haptic property, which is of great use in environments where a direct operator contact is deemed to be lethal or risky and the operator cannot keep watch on the distant end-effector. The telerobotics and the environment are simulated by the haptic virtual system that enables the operator to feel the actual force feedback from the virtual environment just as they would from the real environment. The reaction forces from the virtual environment are felt by the operator through a feedback control scheme. This allows operators to be located in a safe area and to control the distant manipulator with a virtual image and duplicate on-line the motion of the distant processes quickly and accurately, so that they can feel the actual environment or the conditions of operation. However, it is well known that operator adaptability to the environment and to the conditions of operation is vital for a smooth operation. One way to cope with the problem is to let the operator intervene in the system from a safe distance by means of a controller, and to be part of the overall closed-loop control system. Takahashi and Ogata [5] studied the teleoperation and human machine interfaces and simulated a robotic system using VR technology. In general, robot manipulators have been used by the manufacturing industries for performing certain automation tasks, or used as a master/slave type manipulator in teleoperation. They require an accurate model description for designing the stabilizing controllers. In particular, hand controllers for creating various forces have been designed for maneuvering the remote side of the slave manipulator [6]. It is seen that the performance can be improved significantly by providing force feedback information from the remote site of the virtual environment to the master. Li and Wang [7] modeled force/torque sensing for a working environment using physical based components (e.g. mass and spring/damper) in the VR simulating system. However, an in-depth study of system stability analysis and the implementation of stabilizing controllers in a VR system are still lacking.

In addition, for the haptic "master-slave" telerobotic systems in [8], the operator manipulated an X-Y Table (Master) Robot as a virtual cutting tool and cut a virtual clay, and the operator can feel the force feedback when cutting occurred in the virtual environment. This is very similar to that we operate the joystick (Master) in this research, where the motion simulator is our slave robot. In [9], the player can use a direct-drive robot as a paddle and play ping-pong in a virtual environment. The feeling of force feedback comes from the setting of ball's mass and coefficient of elasticity in the simulation program. It is worth for us to design a haptic system between the joystick and the virtual simulator.

The aim of this article is to propose a new method about the VR Ratio of the real haptic motion simulator and virtual one (the transfer function between real and virtual motion simulator) as shown in Fig. 1 and Fig. 2, so that we do not need to waste lots of time in

adjust the motion simulator by virtual environment anymore; and introduce how to use the motion simulator with a limited space to simulate an unlimited virtual environment, and discuss the relationships with acceleration, velocity, displacement, and the haptic device, virtual environment and the motion simulator.

The whole system combines the master-slave remote control robotic system (the motion simulator and joystick/haptic interface device), the virtual reality system (force feedback joystick and image/sound system), the VR Ratio of the real haptic motion simulator and virtual one, and these dynamic subsystems form a complex multiple bilateral problem of control.

Virtual Reality combines human's feeling with machine that we call "Man Machine Interface". Human operators can make interactions with virtual reality systems through the sense of sight, hearing, touch and action. Because of the fast development of computer technology and haptic device, virtual reality has been used in various applications, e.g. entertainment, education, medical science, military, flight simulation, remote manipulation of mission, and many kinds of training. These make virtual reality becomes an inter-discipline research topic. There is no denying that the applications of virtual reality are unlimited, and the designer's imagination is one of the most important elements to make creation come true.

Human operators will immerse in virtual environment through the Man Machine Interface. It is different from virtual reality and generally multimedia, because we do not only watch but just think that everything is true!

2. Constructions

Our object studied is a 6-SPS pneumatic parallel manipulator driven by air, shown in **Fig. 1**. Its structure is a typical Stew-art platform. The upper and lower platforms of the parallel manipulator are non-equilateral and symmetric hexagons, where the lower platform is fixed and the upper platform can carry out movements with six degrees of freedom within its work-space. There are six actuating links with the same structures and strokes are used to connect the upper and lower platforms via universal joints. A mechanism coordinate of the 6-SPS parallel manipulator is depicted as Fig. 2, based on an analysis of the structure. A moving coordinate system O-XYZ is built on point b_1 of the upper platform, while a fixed coordinate system O-XYZ is built on point B_1 of the lower platform. Any vector $R^{'}$ in a moving coordinate system can be transformed into R in a fixed coordinate system through a transformation of coordinates according to the following equation:

$$R = TR^{'} + P \qquad (1)$$

Where T is a directional cosine matrix of the pose of the upper platform and P is a positional vector from the origin of the moving coordinate system located in the fixed coordinate system.

Fig. 1. A 6-SPS pneumatic parallel manipulator.

In this section, the inverse kinematics and forward kinematics of the parallel robot are studied. Before controlling a robot, it is important and necessary to obtain the inverse and the forward kinematics to handle the position control and path configuration.

The kinematics and inverse kinematics is important and needed when we want to do position control or path configuration. And we also can derive the Jacobian matrix from the velocity equation to judge the singular position.

2.1 Inverse Kinematics

First we can define two coordinate: A fixed reference frame O-XYZ is attached to the base of the mechanism, and a moving coordinate frame O'-$x'y'z'$ is attached to the platform. Point O is located at the center of the base. Moreover, the points of attachment of the actuated arms to the base are designated as Oj, with j=1,..,3, and the points of attachment of all following rods to the platform are described as $\mathbf{P_i}$, with i=1,..,6.

The inverse kinematics of the parallel mechanism is unlike the serial mechanism, we can't find the inherent formula. Hence we use the geometric vector to derive the inverse kinematics of the parallel mechanism. First we set that the coordinates of point Pi in the moving frame are noted $(a_i \quad b_i \quad c_i)$ and the coordinates of point $\mathbf{Oi}$ in the fixed frame are noted $(x_{i0} \quad y_{i0} \quad z_{i0})$ then one has:

$$P_i = \begin{bmatrix} x_i \\ y_i \\ z_i \end{bmatrix} \qquad P_i' = \begin{bmatrix} a_i \\ b_i \\ c_i \end{bmatrix} \qquad P = \begin{bmatrix} x \\ y \\ z \end{bmatrix} \qquad \text{f o } \dot{r} = 1,...,6. \qquad (2)$$

(see Fig. 2) where $\mathbf{P_i}$ is the position vector of point $\mathbf{P_i}$ expressed in the fixed coordinate frame, $\mathbf{P'_i}$ is the position vector of point $\mathbf{P_i}$ expressed in the moving coordinate frame, and $\mathbf{P}$ is the position vector of point $\mathbf{O'}$ expressed in the fixed frame.
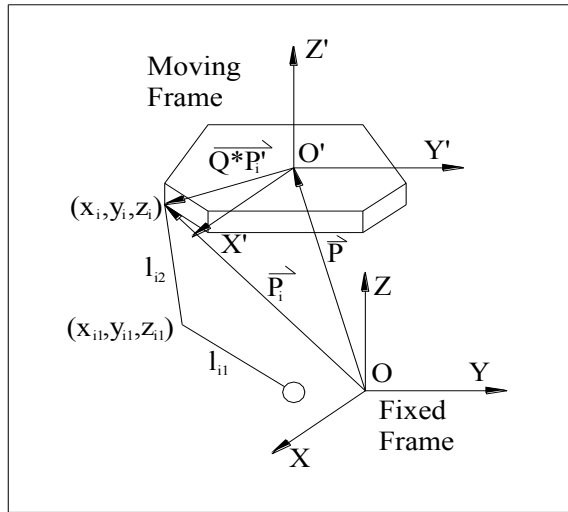
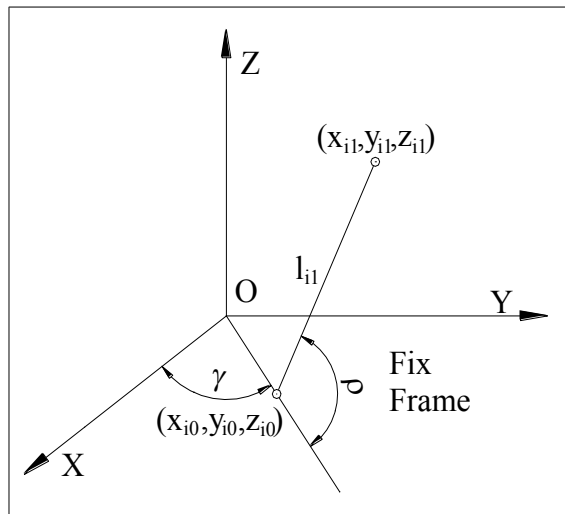**Fig. 2**. The Symbol Mark of the Inverse Kinematics

Fig. 3. The Symbol Mark of the Actuated Arm

One can write:

$$P_i = P + Q \times P'_i \quad \text{for } i = 1,...,6. \tag{3}$$

where Q is the rotation matrix corresponding to the orientation of the platform of the mechanism with respect to the base coordinate frame. In this case, the rotation matrix is unit matrix.

Next, point O'$_i$ is defined as the center of the universal joint connecting the two moving links of the ith actuated rod. Moreover, the Cartesian coordinates of point O'$_i$ expressed in the fixed coordinate frame are noted (x_{i1}, y_{i1}, z_{i1}). (see **Fig. 3**) One can write:

$$x_{i1} = x_{i0} + l_{i1} \times \cos \rho_i \times \cos \gamma_i \tag{4}$$

$$y_{i1} = y_{i0} + l_{i1} \times \cos \rho_i \times \sin \gamma_i \tag{5}$$

$$z_{i1} = z_{i0} + l_{i1} \times \sin \rho_i \tag{6}$$

where γ_i is the angle between the positive direction of the x axis of the base coordinate frame and the axis of ith actuated joint, and ρ_i is the joint variable associated with the ith actuated arm. Moreover, l_{i1} is the length of the first link of the ith actuated arm. From the geometry of the mechanism, one can write:

$$(x_i - x_{i1})^2 + (y_i - y_{i1})^2 + (z_i - z_{i1})^2 = l_{i2}^2 \quad \text{for } i = 1,...,6. \tag{7}$$

Substituting Eqs.(3), (4), (5), (6) into Eq.(7), one obtains:

$$R_i \times \cos \rho_i + S_i \times \sin \rho_i = T_i \quad \text{for } i = 1,...,6. \tag{8}$$

$$R_i = (y_i - y_{i0}) \times \cos \gamma_i + (x_i - x_{i0}) \times \sin \gamma_i \tag{9}$$

$$S_i = Z_i - Z_{i0} \tag{10}$$

$$T_i = \frac{(x_i - x_{i0})^2 + (y_i - y_{i0})^2 + (z_i - z_{i0})^2 + l_{i1}^2 - l_{i2}^2}{2l_{i1}} \tag{11}$$

which leads directly to

$$\sin \rho_i = \frac{S_i T_i + K_i R_i \sqrt{V_i}}{R_i^2 + S_i^2} \quad \text{for } i = 1,...,6. \tag{12}$$

$$\cos \rho_i = \frac{R_i T_i - K_i S_i \sqrt{V_i}}{R_i^2 + S_i^2} \quad \text{for } i = 1,...,6. \tag{13}$$

$$K_i = \pm 1, V_i = R_i^2 + S_i^2 - T_i^2 \quad \text{for } i = 1,...,6. \tag{14}$$

$$\rho_i = a \tan 2[\sin \rho_i, \cos \rho_i] \quad \text{for } i = 1,...,6. \tag{15}$$

where *atan2* denotes the inverse tangent function, which returns a unique value based on the signs of the sine and cosine arguments.

Since two solutions are obtained for each of the ρ i's, it is clear that the inverse kinematics problem of this mechanism leads to 8 solutions, which can be distinguished by using branch indices Ki.

2.2 Jacobian

The velocity equation of the mechanism are important for their kinematic analysis. Indeed, since the velocity equations represent the linear mapping between the joint velocities and the Cartesian velocities, they characterize the kinematic accuracy of a mechanism and they allow the determination of the singularities.

Differentiating Eq.(8) with respect to time, one obtains:

$$\dot{R}_i \times \cos \rho_i - R_i \times \sin \rho_i \times \dot{\rho}_i + \dot{S}_i \times \sin \rho_i + S_i \times \cos \rho_i \times \dot{\rho}_i = \dot{T}_i \qquad (16)$$

The Eq.(16) can become:

$$\dot{\rho}_i \times (S_i \times \cos \rho_i - R_i \times \sin \rho_i) = \dot{T}_i - \dot{R}_j \times \cos \rho_i - \dot{S}_i \times \sin \rho_i \qquad (17)$$

$$\dot{R}_i = \cos \gamma_i \times \dot{y}_i - \dot{x}_i \times \sin \gamma_i \qquad (18)$$

$$\dot{S}_i = \dot{z}_i \qquad (19)$$

$$\dot{T}_i = \frac{2(x_i - x_{i0})\dot{x}_i + 2(y_i - y_{i0})\dot{y}_i + 2(z_i - z_{i0})\dot{z}_i}{2l_{i1}} \qquad (20)$$

From Eqs.(16), (17), (18), (19), one obtains:

$$\begin{aligned}
l_{i1}(S_i \times \cos \rho_i - R_i \times \sin \rho_i)\dot{\rho}_i &= (x_i - x_{i0} + l_{i1} \times \sin \gamma_i \times \cos \rho_i)\dot{x}_i \\
&\quad + (y_i - y_{i0} - l_{i1} \times \cos \gamma_i \times \cos \rho_i)\dot{y}_i \\
&\quad + (z_i - z_{i0} - l_{i1} \times \sin \rho_i)\dot{z}_i
\end{aligned} \qquad (21)$$

Differentiating Eq.(21) with respect to time, one obtains:

$$\dot{x}_i = \dot{x}, \dot{y}_i = \dot{y}, \dot{z}_i = \dot{z} \qquad (22)$$

Substituting Eq.(22) into Eq.(21), one obtains:

$$\begin{aligned}
l_{i1}(S_i \times \cos \rho_i - R_i \times \sin \rho_i)\dot{\rho}_i &= (x_i - x_{i0} + l_{i1} \times \sin \gamma_i \times \cos \rho_i)\dot{x} \\
&\quad + (y_i - y_{i0} - l_{i1} \times \cos \gamma_i \times \cos \rho_i)\dot{y} \\
&\quad + (z_i - z_{i0} - l_{i1} \times \sin \rho_i)\dot{z}
\end{aligned} \qquad (23)$$

We can show Eq.(23) as:

$$B_r \times \dot{\rho} = K_r \times \dot{X} \tag{24}$$

where

$$B_r = \begin{bmatrix} b_1^r & 0 & 0 \\ 0 & b_2^r & 0 \\ 0 & 0 & b_3^r \end{bmatrix} \quad K_r = \begin{bmatrix} k_{11}^r & k_{12}^r & k_{13}^r \\ k_{21}^r & k_{22}^r & k_{23}^r \\ k_{31}^r & k_{32}^r & k_{33}^r \end{bmatrix} \tag{25}$$

$$b_i^r = l_{i1} \times (S_i \times \cos \rho_i - R_i \times \sin \rho_i)$$
$$k_{i1}^r = x_i - x_{i0} + l_{i1} \times \sin \gamma_i \times \cos \rho_i$$
$$k_{i2}^r = y_i - y_{i0} - l_{i1} \times \cos \gamma_i \times \sin \rho_i$$
$$k_{i3}^r = z_i - z_{i0} - l_{i1} \times \sin \rho_i \quad \text{for } i = 1,...,3.$$

We set the parameters as:

$$\dot{\theta} = \begin{bmatrix} \dot{\rho}_1 \\ \dot{\rho}_2 \\ \dot{\rho}_3 \end{bmatrix} \qquad \dot{X} = \begin{bmatrix} \dot{x} \\ \dot{y} \\ \dot{z} \end{bmatrix} \tag{26}$$

Substituting Eq.(26) into Eq.(24), one obtains:

$$\dot{X} = K_r^{-1} B_r \dot{\theta} \tag{27}$$

$$J = K_r^{-1} B_r \tag{28}$$

Eq.(27) is the velocity equation of the parallel mechanism and the Jacobian matrix is shown as Eq.(28).

2.3 Forward Kinematics

The kinematics as the same as the inverse kinematics can not find the inherent formula and it is more difficult to derive. We still use geometric vector to derive the kinematics of the parallel mechanism. First we define five coordinate frames:
- The moving coordinate frame O'-x'y'z' (M coordinate frame).
- The fixed reference frame O-xyz (F coordinate frame).
- F_1 coordinate frame: its origin fixed at motor's axis and $x_{(F1)}$ axis parallels the motor's axis and $z_{(F1)}$ axis is perpendicular to the base.
- F_2 coordinate frame: its origin fixed at the center of the universal joint and three axis's directions is the same as the F_1 coordinate frame.
- F_3 coordinate frame: its origin fixed at the center of the universal joint and $y_{(F3)}$ axis overlaps with the $y_{(F2)}$ axis.
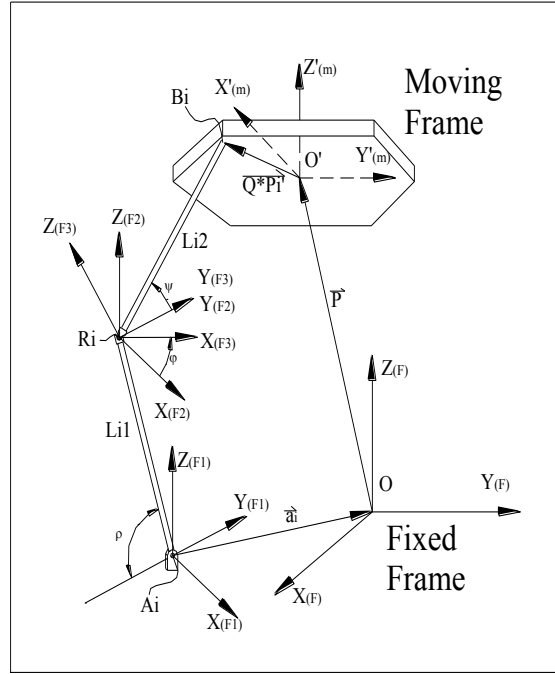
Fig. 4. The Symbol Mark of the Forward Kinematics

From **Fig. 4**, we know:

$$\overrightarrow{A_iB_{i(F)}} = \overrightarrow{A_iR_{i(F)}} + \overrightarrow{R_iB_{i(F)}} = -\mathbf{a}_{i(F)} + \mathbf{P}_{i(F)} + \mathbf{Q} \times \mathbf{P'}_{i(M)} \tag{29}$$

Now we hypothesize the following rod that rotates about the y(F3) axis in the F3 coordinate frame, one obtains:

$$\overrightarrow{R_iB_{i(F3)}} = \begin{bmatrix} 0 & l_{i2} \times \cos\psi_i & l_{i2} \times \sin\psi_i \end{bmatrix}^T \tag{30}$$

Then we hypothesize the F_3 coordinate frame that rotates φ angle about the $y_{(F2)}$ axis with respect to F_2 coordinate frame, so the rotation matrix is :

$$\mathbf{Q_i}_{F3 \to F2} = \begin{bmatrix} \cos\varphi_i & 0 & -\sin\varphi_i \\ 0 & 1 & 0 \\ \sin\varphi_i & 0 & \cos\varphi_i \end{bmatrix} \tag{31}$$

$$\overrightarrow{R_iB_{i(F1)}} = \overrightarrow{R_iB_{i(F2)}} = \mathbf{Q_i}_{F3 \to F2} \times \overrightarrow{R_iB_{i(F3)}} \tag{32}$$

The $\overrightarrow{AB}$ vector in F_1 coordinate frame is:

$$\overrightarrow{A_iB_{i(F1)}} = \overrightarrow{A_iR_{i(F1)}} + \overrightarrow{R_iB_{i(F1)}} \tag{33}$$

$$\overrightarrow{A_iR_{i(F1)}} = \begin{bmatrix} 0 & -l_{i1} \times \cos\rho_i & l_{i1} \times \sin\rho_i \end{bmatrix}^T \tag{34}$$

The rotation matrix that F_1 coordinate frame with respect to F coordinate frame is:

$$\underset{F1\to F}{\mathbf{Q_i}} = \begin{bmatrix} -\sin\gamma_i & -\cos\gamma_i & 0 \\ \cos\gamma_i & -\sin\gamma_i & 0 \\ 0 & 0 & 1 \end{bmatrix} \tag{35}$$

From Eq.(29), one obtain:

$$\overrightarrow{A_iB_{i(F)}} = \underset{F1\to F}{\mathbf{Q_i}} \times \overrightarrow{A_iB_{i(F1)}} = -\mathbf{a_i} + \mathbf{P}_{(F)} + \mathbf{Q} \times \mathbf{P'}_{\mathbf{i}(M)} \tag{36}$$

Substituting Eqs.(30), (31), (32), (33) into Eq.(34), one obtains:

$$\begin{bmatrix} l_{i2} \times \sin\varphi_i \times \sin\psi_i \times \sin\gamma_i - l_{i2} \times \cos\psi_i \times \cos\gamma_i + l_{i1} \times \cos\rho_i \times \cos\gamma_i \\ -l_{i2} \times \sin\varphi_i \times \cos\gamma_i \times \sin\psi_i - l_{i2} \times \cos\psi_i \times \sin\gamma_i + l_{i1} \times \cos\rho_i \times \sin\gamma_i \\ l_{i1} \times \sin\rho_i + l_{i2} \times \cos\varphi_i \times \sin\psi_i \end{bmatrix} \tag{37}$$
$$= -\mathbf{a_i} + \mathbf{P} + \mathbf{Q} \times \mathbf{P'}_{\mathbf{i}} \quad \text{for } i = 1,...,6.$$

From Eq.(37), it will get 9 equation and 9 unknown, we can use numerical method to solve this unknown.

3. System Description

In order to simulate an unlimited space in virtual environment, we should create a new way to make it possible. Although the motion simulator has a limited space, we can define a filter to determine the maximum movement of the motion simulator to limit its maximum moving range. All these conditions are based on a situation that if acceleration occurs in the virtual environment, then the human on the motion simulator should feel acceleration as well. Owing to the limited space of the motion simulator, if the virtual environment undergoes a uniform velocity, the chair on the motion simulator will be back to the original place. Due to the different space between the motion simulator and the virtual environment, we can divide it into three cases:

$$\text{Case1}: \left| \frac{Virtual}{Space} \right| = \left| \frac{\text{Re}\,ality}{Space} \right| \doteqdot \text{K=1}$$

Case2：$\boxed{\dfrac{Virtual}{Space}} = \alpha \boxed{\dfrac{\text{Re}\,ality}{Space}} \doteqdot \dfrac{1}{\alpha}$

Case3：Unlimited $\boxed{\dfrac{Virtual}{Space}} = \boxed{\dfrac{\text{Re}\,ality}{Space}} \doteqdot$ K=?

Assume that the proportion of virtual space and reality space is *K*, it means if the virtual space is unlimited and the reality space is limited (maximum length of the motion simulator), we could obtain the range of value *K* and try the best value to get better feeling of the operator.

Our feelings contain lots of sense and consciousness. Among which sense of sight comes from variation of virtual environment, and sense of moving comes from the motion simulator just like Fig. 3. Human operator can feel *1:1* acceleration and displacement between sense of sight and virtual environment. But sense of moving will appear K-fold relation with the motion simulator and must be in the same phase.
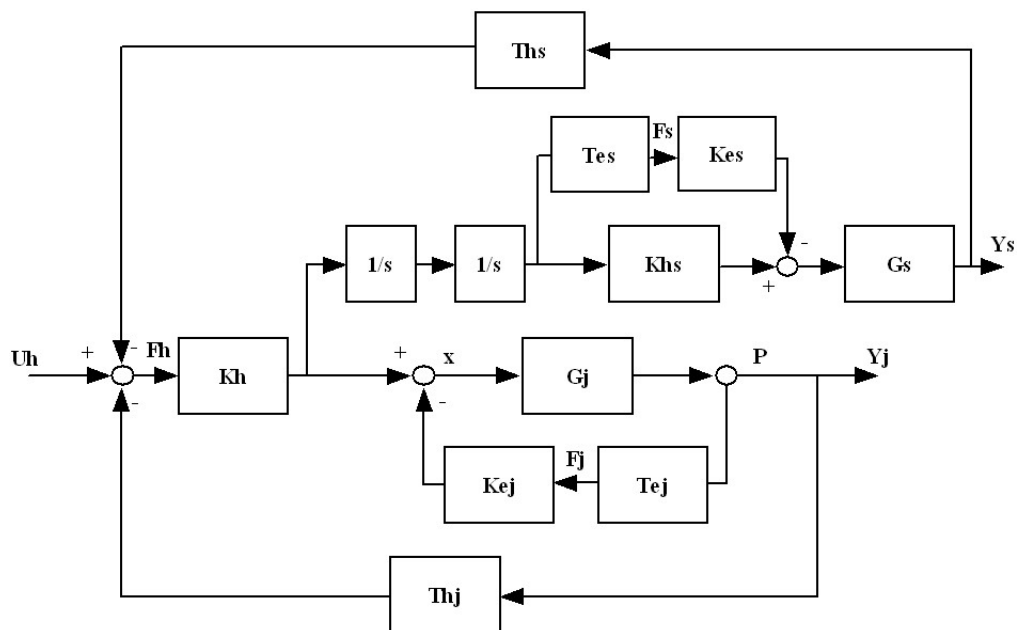

Fig. 5. System Frame

The diagram of the multiple bilateral control system is shown in **Fig. 5**. The operator can feel force feedback from Thj by joystick and Ths by the motion simulator. Gs and Gj are the close-loop controllers. Tej and Tes are the transfer functions of virtual environment dynamics; Kej and Kes are the compensator transfer functions for Fj and Fs. Tej, Tes, Kej, and Kes offer the vision feedback to the operator. Obviously, there are two systems Yj (for joystick) and Ys (for simulator) in the diagram that will interact. This system model includes a bilateral control interface between two haptic devices and a virtual environment.
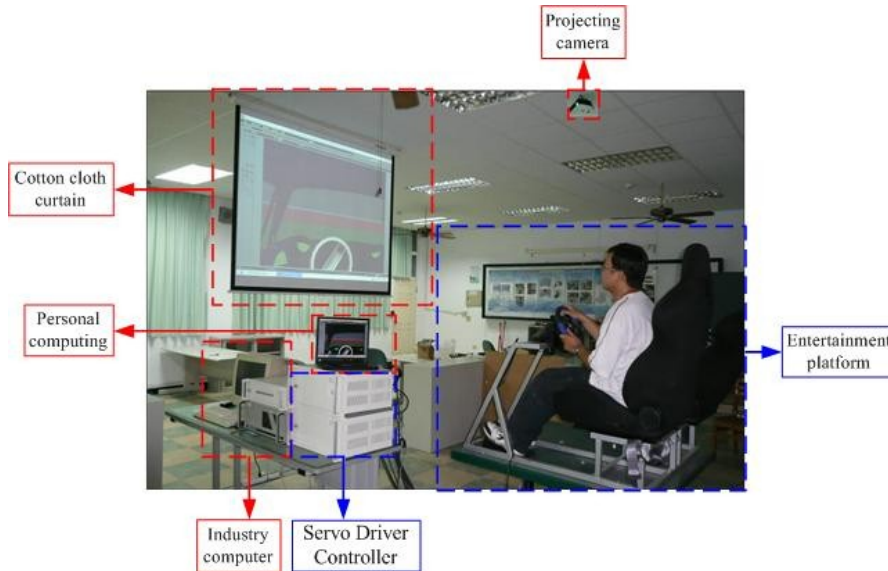
Fig. 6. 6-axis motion simulator for space entertainment system

In **Fig. 6**, when the operator manipulates the joystick, he would receive force feedback from the joystick, and moving feeling from the motion simulator, and vision from virtual environment. In the meantime, velocity data of the joystick would be sent to virtual environment. Then the motion simulator will move according to the calculated data through $\dfrac{Ks}{s+a}$ which is the transfer function Khs in **Fig. 5**. However, if the motion simulator moves acutely, it will let the joystick sway. In this case, it is assumed that the operator is on the motion simulator and holds the joystick. It means the operator's body is like a shock absorber which won't let the joystick keep shaking. Hence, it is needed to adjust the gains K and a to remove these noise, otherwise the reciprocal effects of the shaking joystick and moving simulator will make the whole system unstable.

3.1 Acceleration of Virtual Environment and the Motion Simulator

Based on this conception, this article assumes that joystick's variation of displacement represents velocity of virtual environment. We set a transfer function $\left(\dfrac{Ks}{s+a}\right)$ between the motion plat and virtual environment, just like a filter. Now, if we accelerate the speed gradually, that means joystick is moved slowly, so the low frequency makes s very small, $\left(\dfrac{s}{s+a}\right)$ will approach to zero. At this situation, the chair on the motion plat won't change its displacement, and human operator feels the speed just by sense of sight from virtual environment. If we accelerate the speed instantly, that means joystick is move very fast, so the high frequency makes s very big, $\left(\dfrac{s}{s+a}\right)$ will approach to infinity. Then the motion plat and virtual environment will appear K-fold relation. Acceleration of virtual environment

（ A_V ）：

Consider the system
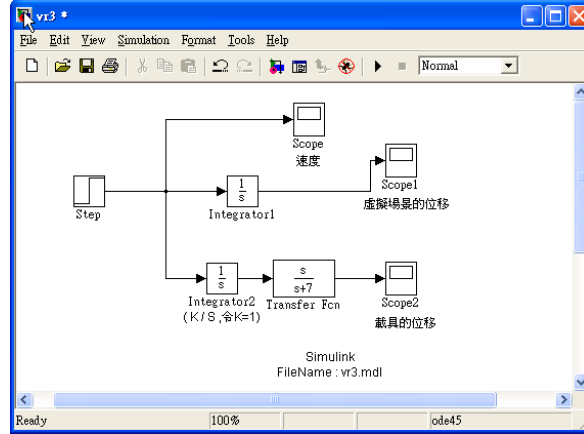
$$V \rightarrow \frac{1}{s} \rightarrow A_V$$

Then

$$A_V = sV \tag{38}$$

Acceleration of the motion plat（ A_R ）：
Consider the system
Acceleration of the motion simulator（ A_R ）：

$$V \rightarrow \frac{K}{s} \rightarrow \frac{s}{s+a} \rightarrow X_n$$
$$V \rightarrow \frac{K}{s} \rightarrow \frac{S}{s+a} \rightarrow s^2 \rightarrow A_R$$

then

$$A_R = \left(s^2\right)\left(\frac{s}{s+a}\right)\left(\frac{K}{s}\right)V = \frac{Ks^2}{s+a}V \tag{39}$$

Hence the ratio of the motion plat and virtual environment：

$$\frac{A_R}{A_V} = K\left(\frac{s}{s+a}\right) \tag{40}$$

In **Fig. 7**, we can simulate the acceleration of vision environment and the acceleration of the motion simulator plat. when High Frequency, s approach to infinity, then $\frac{s}{s+a}$ approach to1 ， $\frac{A_R}{A_V}$ → K-fold（As joystick moves instantly.）

When Low Frequency, S very small, $\frac{s}{s+a}$ approach to zero, $\frac{A_R}{A_V}$ → 0（Human operator feel acceleration by sense of sight.）. In Fig. 4, we can observe that $\frac{A_R}{A_V}$ appears a proportional distribution. And the Bode diagram of $\frac{s}{s+a}$ presents that the magnitude approach to 1 on high frequency; and no matter how the operator accelerates or decelerates that the motion simulator will be in the same phase, that means when the operator accelerates forward with a joystick, the motion simulator won't go back to the opposite direction.
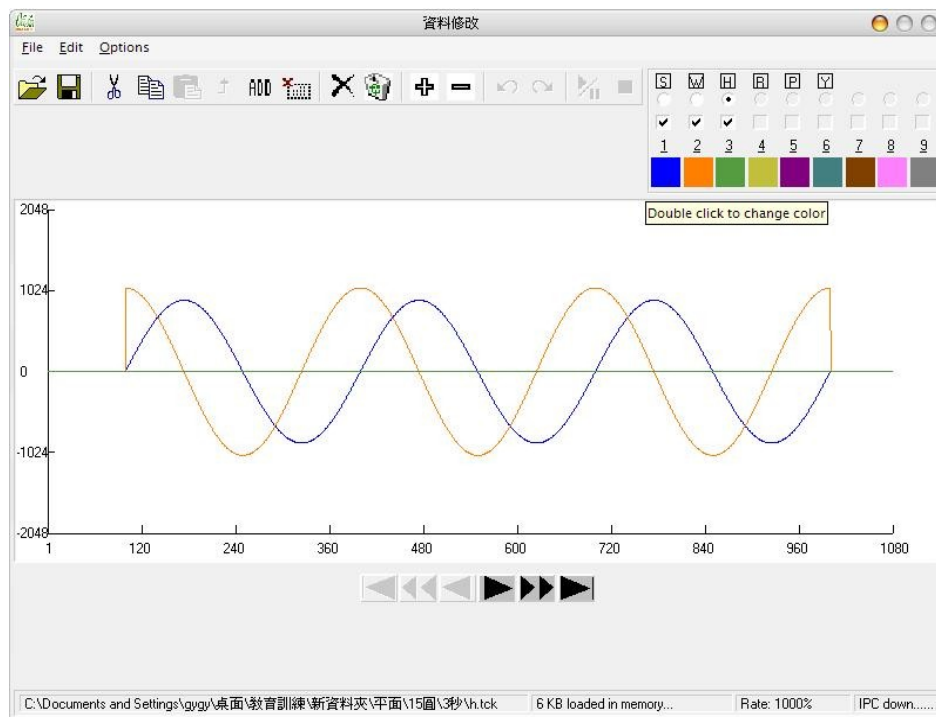

Fig. 7. (left) Acceleration of vision environment, (right) Acceleration of the motion simulator plat
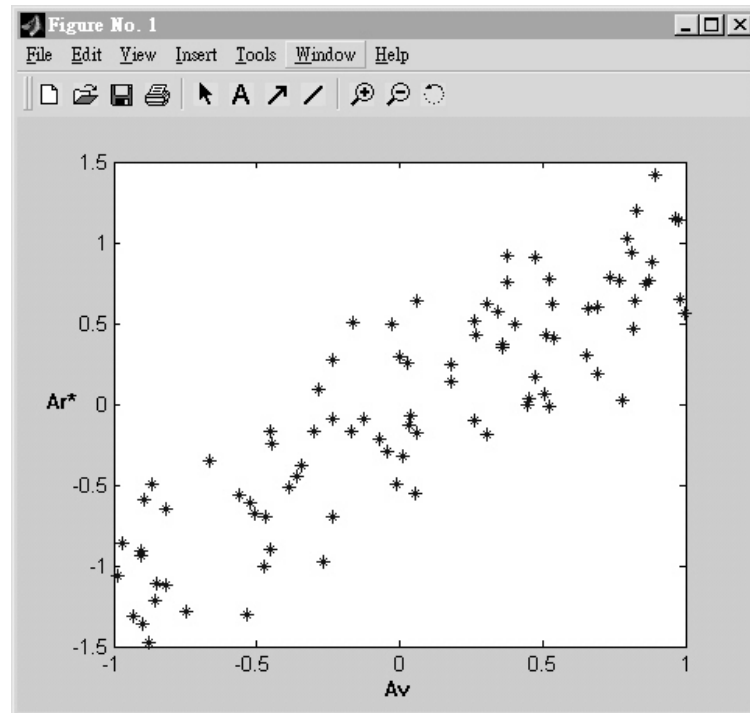
Fig. 8. $\dfrac{A_R}{A_V}$ appears proportional distribution

We set joystick's variation of displacement represents velocity of virtual environment, and this velocity passes through an integrator, it will become displacement of virtual environment. And if it passed through an integrator and a filter $\dfrac{s}{s+a}$ and multiplied by *K*, we could obtain displacement of the motion plat. So, if human operator moves the joystick immediately, the high frequency makes S very big, $\dfrac{s}{s+a}$ will approach to 1. At present, displacement between the motion plat and virtual environment has a *K*-fold relation. In other words, if human operator moves joystick gradually, S will be very small and $\dfrac{s}{s+a}$ will approach to zero, chair on the motion plat won't move, then human operator will feel displacement just by sense of sight.

3.2 Displacement of Virtual Environment and the Motion Simulator

The joystick's variation of displacement is set to the velocity of virtual environment, and this velocity passes through an integrator, in which it will become the displacement of the virtual environment. And if it passed through an integrator and a filter $\dfrac{s}{s+a}$, and also is multiplied by K, we could obtain the displacement of the motion simulator as follows:

$$V \to \frac{K}{s} \to \frac{s}{s+a} \to K_R \Rightarrow V \to \frac{K}{s+a} \to X_R$$

$$\Rightarrow X_R(s) = \frac{K}{s+a}V(s) \tag{41}$$

where

$$V \to V_{max}$$

thus

$$X_R = \frac{K}{s+a}V_{max}(s) \tag{42}$$

$$X_R(s) = \lim_{s \to 0} \frac{K}{s+a}V_{max} = \frac{KV_{max}}{a} \tag{43}$$

We already know that the maximum displacement of the motion simulator is $X_{R\,max}$, then we can calculate K.

3.3 3D aircraft case

This section, we program has two DOF about X-axis(left and right) and Y-axis(accelerate and decelerate). We can control the airplane by keyboard or joystick. When the airplane collides with something in the game, the joystick will vibrate. The flight data about velocity and acceleration are indicated by the program interface. If we consider the resistance of water, we could simulate a submarine system shown as **Fig. 9** and as follow:

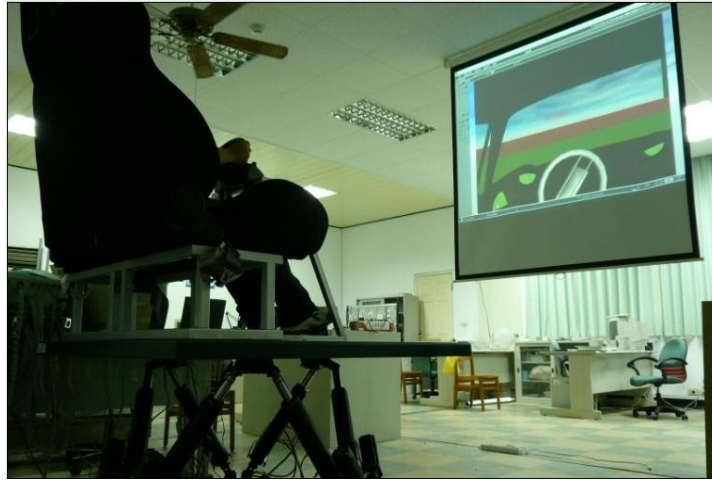$$m\ddot{x} = F - b\dot{x} \tag{44}$$
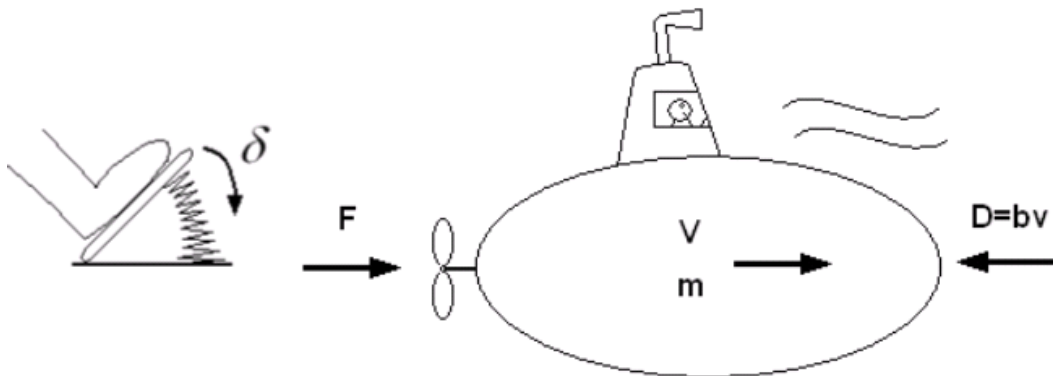
Fig. 9. Submarine

If the throttle is set to accelerate, where

$$F = \kappa\delta \tag{45}$$

Then we can obtain

$$\frac{x(s)}{F(s)} = \frac{1}{ms^2 + bs} \Rightarrow \frac{x(s)}{\delta(s)} = \frac{\kappa}{ms^2 + bs} \tag{46}$$

Therefore, we can derive two system equations that relate the displacement and velocity of submarine with $\delta(s)$.

$$x(s) = \frac{\kappa}{ms^2 + bs}\delta(s) \tag{47}$$

$$V(s) = \frac{\kappa}{ms + b}\delta(s) \tag{48}$$

or expressed in time-domain

$$x(t) = L^{-1}\frac{\kappa}{ms^2 + bs}(\frac{\Delta}{s}) \tag{49}$$

$$V(t) = L^{-1} \frac{\kappa}{ms+b}(\frac{\Delta}{s}) \tag{50}$$

If $t \rightarrow \infty$, then

$$x(t) \rightarrow \infty$$

$$V(t) = \lim_{s \rightarrow 0}(s)(\frac{\kappa}{ms+b})(\frac{\Delta}{s}) = \frac{\kappa\Delta}{b} \tag{51}$$

where $\frac{\kappa\Delta}{b}$ is a terminal velocity.

Besides, because of

$$x_R = (\frac{Ks}{s+a})x \tag{52}$$

where K is a scaling factor.

Thus

$$x_R = \frac{\kappa\delta}{ms^2+bs} \cdot \frac{Ks}{s+a} = \frac{\kappa K\delta}{(ms+a)(s+a)} \tag{53}$$

and the maximum of x_R can be written as

$$x_{R\max} = \lim_{s \rightarrow 0} s \frac{\kappa K}{(ms+b)(s+a)} \frac{\delta_{\max}}{s} = \frac{\kappa K}{ab}(\delta_{\max}) \tag{54}$$
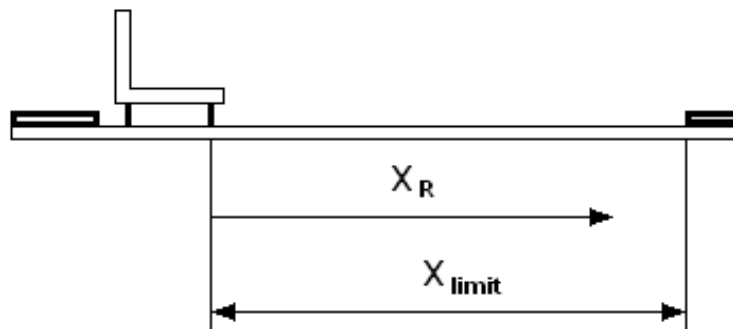
Fig. 10. The real displacement of the chair on the motion simulator

Because of the length limit of the motion simulator, thus

$$x_{R\max} < x_{\lim it}$$

Then

$$\frac{\kappa K \delta_{\max}}{ab} < x_{\lim it} \Rightarrow K < \frac{abx_{\lim it}}{\kappa \delta_{\max}}$$

So when $K = 1$, the human operator will feel the 1:1 reality between the real displacement and the visional displacement.

4.   Experiment

The hardware configuration of the experimental system is illustrated in **Fig. 11**, where it mainly consists of the force feedback joystick, the motion simulator, and the eye-trek. This multiple bilateral control system integrates servo control, mechanical design, dynamic analysis, graphic interface, and virtual reality system. Several experiments are conducted to validate our theoretical developments.
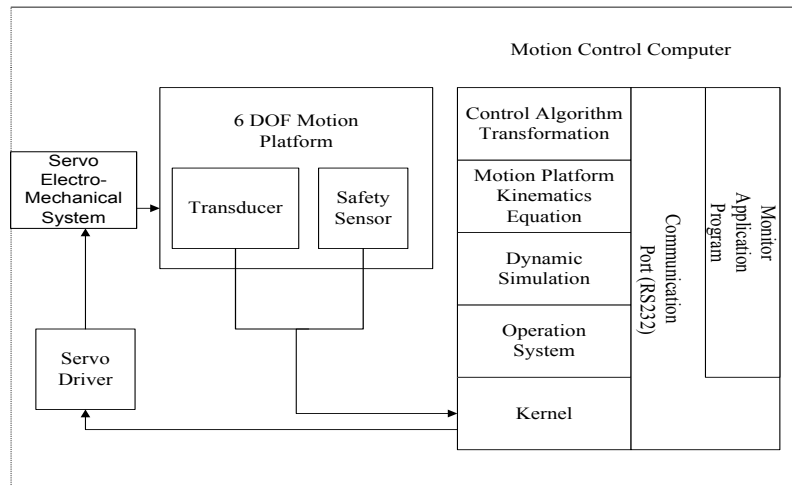

Fig. 11. Hardware configuration of the experimental system

The hardware system in Fig. 11 mainly contents the force feedback joystick, the motion simulator, and the eye-trek. This multiple bilateral control system integrates servo control, mechanical design, dynamic analysis, graphic interface, and virtual reality system. And we design several experiments to validate our theoretical developments.

There are two parts in chief, the first one we discuss is only the property of transfer function $\dfrac{Ks}{s+a}$ simply without calling auto-back function. And we experiment with different K, a, frequency, and operators to obtain the best VR ratio of the real haptic motion simulator and virtual one. The second one is the influence of calling the auto-back function of the system.
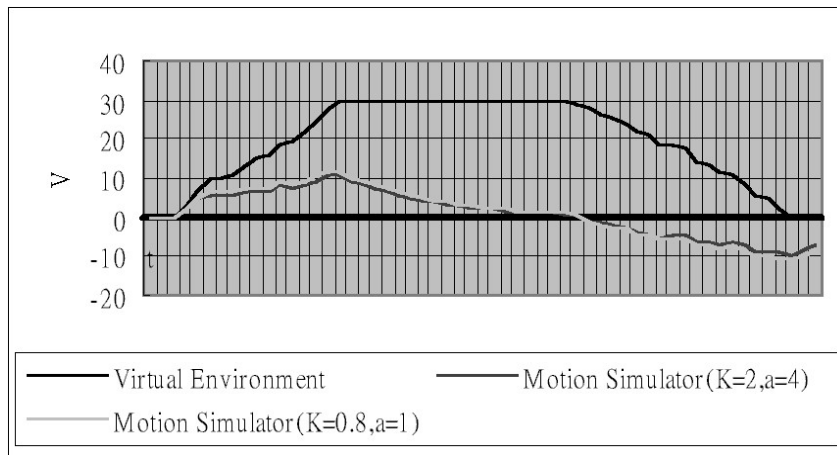
(a)
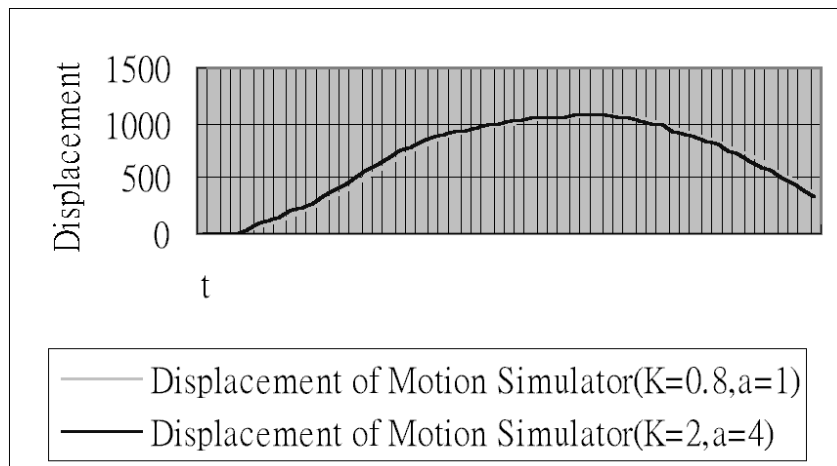
(b)

Fig. 12. On low frequency, **(a)**Velocity of virtual environment and motion simulator, **(b)**Displacement of the motion simulator

In Fig. 12, the system is on low frequency without auto-back function that we can notice the variation of the virtual simulator in virtual environment in (A), and there is a uniform velocity at intermediate zone. We set two situations where $K = 0.8$ and $a = 1$, $K = 2$

and $a = 4$. Because these two situations have better experimental results for feeling of the operator and have lower unstable noise. We can observe that if the operator accelerates slowly, the motion simulator also accelerates slowly but slope is small. When the virtual simulator keeps at uniform velocity, the motion simulator will decelerate until its velocity is equal to zero. Then the operator decelerates slowly, although the virtual simulator still goes forward, the motion simulator moves back instead. Because the property of transfer function $\dfrac{Ks}{s+a}$ simulates the accelerated feeling (direction of force) of human. We can assume that the operator is in a real car. As a car accelerates forward, the operator feels a force backward. So the motion simulator also accelerates forward. If a car decelerates forward, the operator will feel a force forward. The motion simulator decelerates backward instead. The key point is how can we create a best feeling by adjusting value K and a for obscuring the operator to change the moving direction of the motion simulator.

We can obtain the displacement of the motion simulator by integrating its velocity in Fig. 12(B). Although a virtual car still goes forward in the virtual environment, the real displacement of the motion simulator would be back to its original place.

5.   Concluding Remarks

Through $\dfrac{Ks}{s+a}$, we certainly do not need to waste time to adjust the motion simulator by virtual environment anymore, and it simulates the haptic feedback for accelerated feeling of the operator successfully. We can regulate the whole system performance and stability by varying the gains of the transfer function. Then we can obtain and evaluate the effects of simulation swiftly by calculating the VR Ratio.

References

[1] D. K. Boman, "International survey: Virtual-environment research," *Journal of IEEE Computer*, pp.57-65, 1995.
[2] D. S. Kwon, K. Y. Woo and H. S. Cho, "Haptic control of the master hand controller for a microsurgical telerobot system," in *Proc. of the 1999 IEEE International Conference on Robotics and Automation*, 1999.
[3] B. Hannaford, "A design framework for teleoperators with kinematic feedback," *IEEE Transaction on Robotics and Automation*, 1989.
[4] H. Kazerooni and T. J. Snyder, "Case study on haptic device: human-induced instability in power hand controllers," *Journal of Dynamic Systems, Measurement and Control*, 1995.
[5] T. Takahashi and H. Ogata,"Generating and replanning robot commands based on human operation," *Journal of Japen Society for Artificial Intelligence*, pp.448-455, 1994.
[6] D. A. Mcaffee and P. Fiorini, "Hand controller design requirements and performance issues in telerobotics," in *Proc. of International Conference on Advanced Robotics*, pp.186-192, 1991.
[7] Y. F. Li and J. G. Wang, "Incorporating sensing in virtual environment for robotic tasks," *IEEE Instrumentation and Measurement Technology Conference*, 1998.
[8] Ming-Guo Her, Kuei-Shu Hsu, and Tian-Syung Lan, "Virtual Reality Application for Direct Drive Robot with Force Feedback," *Journal of Advanced Manufacturing Technology*, 2003.
[9] Ming-Gou Her and Kuei-Shu Hsu and M. Karkoub, "Design and Analysys of a Direct-Drive Haptic Interface Device for Virtual Reality Applications," *Journal of Intelligent & Robotic Systems*, No. 35, pp. 247-264, 2002.

Kuei-SHu Hsu received his M.S. degree in mechanical engineering and Ph.D. degree in automation control group of the mechanical engineering from Tatung University, in 1997 and 2001, respectively. From 2001 to 2004 he was an Assistant Professor, and from 2005 to 2006 Associate Professor in mechanical and automation Engineering at Kao Yuan University. In 2006 he served as the Chairman of the mechanical and automation Engineer. Currently he is an Associate Professor and Chairman of the Department of Applied Geoinformatics, Chia Nan University of Pharmacy & Science. His research interests in design manufacture and command of Man-machine integrated system.

Wei-Ting Cho received the M.S. degrees in Computer Science and Information Engineering from National Cheng Kung University in 2008. He is currently a Ph.D. student in Department of Engineering Science at National Cheng Kung University. His research interests are information retrieval, information extraction, data mining, and embedded system. Before pursuing a Ph.D., he had worked in industry for 2 years.

Chin-Feng Lai received the Ph.D. degree in department of engineering science from the National Cheng Kung University, Taiwan, in 2008. His research interests include multimedia communications, sensor-based healthcare and embedded systems. He is also a project leader of several international, industrially-funded multimedia projects. Now he is making efforts to publish his latest research in the IEEE Transactions on multimedia and the IEEE Transactions on circuit and system on video Technology. He is also a member of the IEEE as well as IEEE Circuits and Systems Society and IEEE Communication Society.

Xiaofei Wang is a Ph.D candidate in the School of Computer Science and Engineering (CSE) at Seoul National University (SNU), Korea. He received the B.S. degree in the Department of Computer Science and Technology of Huazhong University of Science and Technology (HUST) in 2005 and M.S. degree from the School of CSE at SNU in 2008. His current research interests are in the areas of multi-path routing protocol, traffic analysis and service evaluation in wireless mobile networks.

Yueh-Min Huang is a Distinguished Professor in the Department of Engineering Science, National Cheng-Kung University, Taiwan, R.O.C. His research interests include wireless networks, artificial intelligence, and e-Learning. He received his M.S. and Ph.D. degrees in Electrical Engineering from the University of Arizona in 1988 and 1991 respectively. He has co-authored 2 books and has published over 140 refereed journal research papers. Dr. Huang has received many research awards, such as the Best Paper Award of 2007 IEA/AIE Conference, Best Paper Award of the Computer Society of the Republic of China in 2003, the Awards of Acer Long-Term Prize in 1996, 1998, and 1999, Excellent Research Awards of National Microcomputer and Communication Contests in 2006.